Ab initio electronic-structure calculations on the Nb/Zr multilayer system

H. v. Leuken and A. Lodder
Natuurkundig Laboratorium, Vrije Universiteit, Postbus 7161, NL-1007 MC Amsterdam, The Netherlands

M. T. Czyżyk, F. Springelkamp, and R. A. de Groot
Research Institute of Materials, Katholieke Universiteit Nijmegen, Toernooiveld 1, NL-6525 ED Nijmegen, The Netherlands

(Received 20 July 1989)

Ab initio electronic-structure calculations are performed for the Nb/Zr metallic multilayer system in the coherent bcc structure and in the incoherent bcc/hcp structure, observed for small and larger modulation wavelengths, respectively. A new calculational scheme, the localized-spherical-wave method, has been used. This method is optimized for handling large unit cells since it avoids laborious lattice summations. For the coherent structure a range of 1 to 6 monolayers for each metal is considered. The results for the incoherent structure are restricted to 5 monolayers per constituent metal. A model for the Nb/Zr incoherent bcc/hcp unit cell is given, including a relaxed structure at the interface, which leads to 55 atoms inside the unit cell. The measured modulation-wavelength dependence of the electronic specific-heat coefficient γ and the superconducting transition temperature T_c are explained in terms of the calculated results for the density of states. Furthermore, the coherent to incoherent structural phase transition is in agreement with the modulation-wavelength dependence of the total energies. The effects of multilayering both on the density of states and the band structure are traced by comparing the results with those for the constituent pure metallic systems.

I. INTRODUCTION

Artificially made metallic multilayers form a class of materials allowing for the combination and optimization of physical properties. Besides this, completely new properties, such as the supermodulus effect,[1] can also arise. With the advance of multilayer (ML) synthesizing techniques these new materials have become an important subject for both fundamental and technical studies. As a consequence the number of metallic multilayer systems actually realized is rapidly increasing[2,3] and along with this theoretical interest is developing. Electronic-structure calculations of these systems are still scarce, however,[4-7] although it has been shown in the past that they can be very useful in explaining and predicting material properties.

In this work we present electronic-structure calculations of coherent and incoherent Nb/Zr multilayers, which have been the subject of detailed experimental investigation.[8-10] The Nb/Zr multilayer system has a number of interesting features. The electronic specific-heat coefficient[8] γ and the superconducting transition temperature[9] T_c were measured as functions of the modulation wavelength Λ. Both quantities are related to the density of states at the Fermi energy, $N(E_F)$. Furthermore, a structural phase transition has been observed[10] for the Zr part of the ML. The small-Λ multilayers have an overall bcc (110) modulation direction, which means that Zr has adopted its high-temperature bcc structure. This coherency of Zr with Nb is lost for $\Lambda \geq 31$ Å, in that the Zr part of the ML has resumed its low-temperature hcp structure. We will try to relate this behavior to the calculated total energy.

Electronic-structure calculations were performed for the coherent Nb/Zr multilayers, to be denoted as NbZr n:m, for $n=m$, with n ranging from 1 to 6, and for the incoherent NbZr 5:5 system. The localized-spherical-wave method is used, being a modification of the augmented-spherical-wave method[11] in which the basis set is transformed into the most localized one.

The paper is organized as follows. Although the localized-spherical-wave method has already been used previously,[12-16] it has not been described yet. This will be done in Sec. II. Section III is devoted to the determination of the unit cells of the calculated multilayers and the incoherent interface. The results of the electronic-structure calculations are presented and discussed in Sec. IV, including a scheme to interpret the electron energy bands of the coherent multilayers. Conclusions are given in Sec. V.

II. THE LOCALIZED-SPHERICAL-WAVE METHOD

The localized-spherical-wave (LSW) method belongs to a class of variational methods designed to solve the one-electron Schrödinger equation for a solid:

$$[-\nabla^2+V(\mathbf{r})-\varepsilon]\psi(\mathbf{r},\varepsilon)=0\ , \tag{1}$$

in which $V(\mathbf{r})$ is the crystal potential in the local-density approximation. The solution $\psi(\mathbf{r},\varepsilon)$ is expanded in the basis set, and apart from the transformation of the basis set, localized spherical waves are equivalent to the augmented spherical waves in the well-known augmented-spherical-wave (ASW) method of Williams, Kübler, and

Gelatt.[11] After a brief description of the basis set in the ASW method we shall look into the idea behind the LSW method and the need for such a new method.

The ASW method employs the Andersen atomic-sphere approximation (ASA) for the description of the electronic potential. In this scheme the crystal potential is represented by spherically averaged potentials inside space-filling atom-centered spheres, which therefore, necessarily, are overlapping. The ASW basis functions are constructed according to this potential division. At each atomic position a spherical wave is centered which is a solution to the free-particle Schrödinger equation for a fixed kinetic energy κ^2. The spherical wave is defined, in the notation of Ref. 11, as

$$H_L(\mathbf{r}) \equiv i^l \kappa^{l+1} Y_L(\hat{\mathbf{r}}) h_l^+(\kappa r) , \tag{2}$$

where L stands for the angular-momentum indices l and m, $Y_L(\hat{\mathbf{r}})$ is a spherical harmonic, and $h_l^+(\kappa r)$ is the outgoing spherical Hankel function.[17] Inside the atomic spheres the Hankel functions are augmented with solutions of the numerically integrated radial Schrödinger equation for the corresponding potential. At the atomic position $\mathbf{R}_\nu$, at which $H_L(\mathbf{r}_\nu)$ is centered, with $\mathbf{r}_\nu \equiv \mathbf{r} - \mathbf{R}_\nu$, this augmentation is straightforward. At other atomic positions $\mathbf{R}_{\nu'}$, $H_L(\mathbf{r}_\nu)$ must be expanded into spherical functions around $\mathbf{R}_{\nu'}$ before the augmentation of $H_L(\mathbf{r}_\nu)$ can be performed. The Hankel function can be expanded into regular spherical waves

$$J_L(\mathbf{r}) \equiv i^l \kappa^{-l} Y_L(\hat{\mathbf{r}}) j_l(\kappa r) \tag{3}$$

as follows:

$$H_L(\mathbf{r}_\nu) = \sum_{L'} J_{L'}(\mathbf{r}_{\nu'}) B_{L'L}(\mathbf{R}_{\nu'} - \mathbf{R}_\nu) \quad \text{with } |\mathbf{r}_{\nu'}| < |\mathbf{R}_{\nu'} - \mathbf{R}_\nu| , \tag{4}$$

where $j_l(\kappa r)$ is a spherical Bessel function,[17]

$$B_{L'L}(\mathbf{R}) = 4\pi \sum_{L''} I_{LL'L''} \kappa^{l+l'-l''} H_{L''}(\mathbf{R}) \tag{5}$$

defines the direct-space structural matrix, and

$$I_{LL'L''} = \int d\hat{\mathbf{r}}\, Y_L(\hat{\mathbf{r}}) Y_{L'}(\hat{\mathbf{r}}) Y_{L''}(\hat{\mathbf{r}}) \tag{6}$$

are Gaunt coefficients. Now $H_L(\mathbf{r}_\nu)$ can be augmented by a solution of the numerically integrated radial Schrödinger equation for the corresponding potential which matches the Bessel function at the surface of the atomic sphere centered at $\mathbf{R}_{\nu'}$. The matching is done by choosing the proper value of energy for which the radial Schrödinger equation is integrated, and the normalization such that value and normal derivative are continuous across the atomic-sphere boundary. Finally, the basis functions have a form of Bloch sums of the central Hankel functions and the expansion (4). The basis functions in the ASW method constructed in this way have the property of being continuous and continuously differentiable linear combinations of solutions of the Schrödinger equation within atomic spheres. Thus the Hamiltonian and overlap matrix elements, occurring in the eigenvalue problem, can be evaluated by direct, however cumbersome, summations.

The method is optimized for the description of the valence bands. Therefore the kinetic-energy parameter κ, which controls the localization of the single outgoing Hankel function, has to be chosen as small in absolute value.[18] The corresponding augmented spherical waves are then very extended and the evaluation of the Hamiltonian and overlap matrix elements involves summation over very many expansions of the type of Eq. (4). For the systems with large unit cells, even when Ewald's summation techniques for periodic lattices are employed, it becomes a substantial computational task. In order to circumvent the problems described above, the single Hankel function centered on a given site is replaced in the LSW method by its superposition (linear combination) with the Hankel functions centered on neighboring sites. This superposition, called from now on a cluster function, has important virtues. It possesses the point-group symmetry of a given site and, what is essential for the discussion here, it is localized within a certain (cluster) radius around the site under concern. In plain terms the Hankel functions centered on the neighboring sites are screening the Hankel function on the central site. This transformation of the basis set was introduced by Andersen and Jepsen,[19] basically for the muffin-tin orbitals. However, the practical aspects are solved differently in the LSW method. The new basis function, $F_L(\mathbf{r}_\nu)$, has the form

$$F_L(\mathbf{r}_\nu) = H_L(\mathbf{r}_\nu) + \sum_{\nu',L'} [C(\nu,L)]_{\nu'L'} H_{L'}(\mathbf{r}_{\nu'}) \quad \text{with } \nu' \neq \nu \text{ and } |\mathbf{R}_{\nu'} - \mathbf{R}_\nu| \leq R_{\mathrm{cl}}^\nu . \tag{7}$$

The remainder of this section is devoted to the determination of the screening coefficients $[C(\nu,L)]_{\nu',L'}$. The cluster formed by the atom ν together with the atoms ν' inside a sphere of the radius R_{cl}^ν centered at the site ν is depicted in Fig. 1.

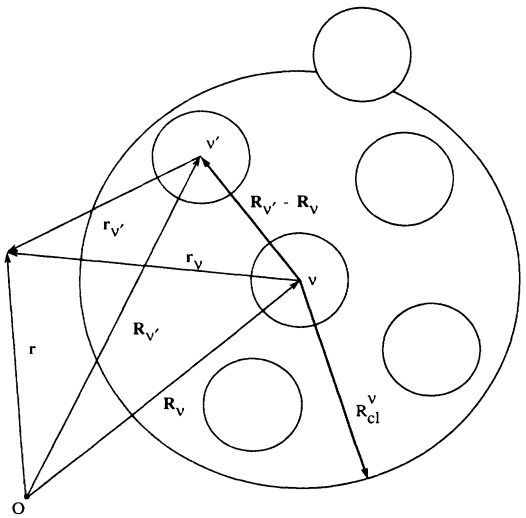

FIG. 1. Hankel functions centered at atoms with positions $\mathbf{R}_{\nu'}$ within a radius R_{cl}^ν around the atom at $\mathbf{R}_\nu$ are used to screen the range of the Hankel functions centered at this position $\mathbf{R}_\nu$. Such a screening procedure is performed for every Hankel function centered inside the unit cell. Hankel functions centered outside the cluster are not considered in the screening procedure.

In order to define the problem of determining the screening coefficients clearly, first the ranges will be specified of the position labels ν and ν' and of the angular momentum labels. The number of clusters to be considered is equal to the number of inequivalent atoms in the unit cell. This determines the range of the variable ν. The number of Hankel functions per cluster to be screened is equal to the size of the basis set on the central atom of the cluster. The size of the basis set is determined the same way as in the ASW and the Andersen linear muffin-tin orbitals (LMTO) methods. For transition metals, as studied in the present paper, functions are used up to $l^{\nu}_{\max}=2$. For rare-earth metals $l^{\nu}_{\max}=3$ has to be used. So, the number of Hankel functions in each cluster which has to be screened out is obviously equal to $(l^{\nu}_{\max}+1)^2$. The number of atoms in the screening cluster $n^{\nu}_{\rm cl}$ is determined by the condition that the central Hankel function is screened to a prescribed accuracy. Given these ranges, the number of degrees of freedom (number of $[C(\nu,L)]_{\nu'L'}$ coefficients) available for screening of a given Hankel function at site ν is

$$D_{\nu}=\sum_{\nu'=1}^{n^{\nu}_{\rm cl}-1}(l^{\nu'}_{\max}+1)^2 . \tag{8}$$

A satisfactory screened behavior of $F_L(\mathbf{r}_{\nu})$ will mean that this function will be negligibly small outside the cluster sphere. Employing the other expansion of the Hankel function,

$$H_L(\mathbf{r}_{\nu})=\sum_{L'}H_{L'}(\mathbf{r}_{\nu'})J_{L'L}(\mathbf{R}_{\nu'}-\mathbf{R}_{\nu}) \quad \text{with } |\mathbf{r}_{\nu'}|>|\mathbf{R}_{\nu'}-\mathbf{R}_{\nu}| , \tag{9}$$

which is complementary to that of (4), and where

$$J_{L'L}(\mathbf{R})=4\pi\sum_{L''}I_{LL'L''}\kappa^{l+l'-l''}J_{L''}(\mathbf{R}) \tag{10}$$

with $I_{LL'L''}$ as defined in Eq. (6), the cluster function for r_{ν} outside the cluster sphere can now be written as

$$F_L(\mathbf{r}_{\nu})=\sum_{L''}H_{L''}(\mathbf{r}_{\nu})\left[\delta_{LL''}+\sum_{\nu',L'}[C(\nu,L)]_{\nu'L'}J_{L''L'}(\mathbf{R}_{\nu}-\mathbf{R}_{\nu'})\right] \tag{11}$$

with the conditions for ν' and $\mathbf{R}_{\nu'}$ the same as in (7). A complete screening of the spherical wave $H_L(\mathbf{r}_{\nu})$ outside the cluster radius $R^{\nu}_{\rm cl}$ means that all coefficients in the large parentheses above should vanish.

The range $l'''^{\nu}_{\max}$ of summation over l'' in the representation (11), emerging from the expansion (9), fixes the number of constraints imposed on the cluster function at that site, and therefore fixes the size of the linear equation set to be solved at the value $(l'''^{\nu}_{\max}+1)^2$. The parameter $l'''^{\nu}_{\max}$ may be interpreted as determining the angular resolution of the representation (11) on the spherical surface of the cluster. Extensive tests for a variety of solids have shown that in order to obtain the required accuracy of screening the number of degrees of freedom D_{ν} is around 150. This means that for $l^{\nu}_{\max}=2$ the typical cluster will include approximately 17 atoms. More atoms are sometimes required in order to maintain the point-group symmetry of the site under consideration. The value of $l'''^{\nu}_{\max}=19$ was found as appropriate for representation (11). Therefore we are faced with the problem to determine about 150 screening coefficients from a set of 400 linear equations. As an efficient, satisfactorily accurate and numerically stable procedure we satisfied the first 100 constraints (until $l''^{\nu}=9$) exactly. The remaining constraints are taken into account by a least-squares method.

This completes the description of the basis set in the LSW method. A few comments are in order here. The transformation of the basis set described above takes place in real space before augmentation. This implies that the procedure is independent of k vector and potentials and needs to be performed only once. The total number of screening coefficients grows linearly with the number of atoms in the unit cell. This leads to manageable data sets to be stored. It is trivial to construct Bloch functions for a given k vector from the localized cluster function. If a screening Hankel function is centered at a position outside the unit cell, related to a unit cell position with the lattice vector $\mathbf{R}$, its screening coefficient and the corresponding coefficients (5) simply enter the unit cell through multiplication with a phase factor $e^{i\mathbf{k}\cdot\mathbf{R}}$. In this way, for large systems, the computational effort will mainly concentrate on the diagonalization. Typical gains in efficiency, compared with the ASW method, are a factor of 3 for four atoms per unit cell and a factor of 6 for 16 atoms per unit cell.

III. STRUCTURE

In this section a description of the crystal structures of the coherent and incoherent Nb-Zr ML systems, as used in our calculations, will be presented.

The coherent systems are experimentally determined[9] to be bcc (110) modulated with a lattice parameter of 3.44 Å. These observations completely determine the structure of a coherent ML. With the z axis defined along the modulation direction, the resulting crystal structure is the C-face-centered orthorhombic (cco) lattice. The structure of the NbZr n:n systems for $n=1$ and 2 is visualized in Fig. 2. In Fig. 2(a) the conventional and primitive cco cells are given for the NbZr 1:1 ML system. The primitive cell is described in this figure by the vectors V_1, V_2, and V_3, of which the latter is in the bcc (110) direction with as length the modulation wavelength Λ. Two extra atoms are drawn that would complete a conventional bcc cell if all the atoms were of the same type. Systems with larger modulation wavelengths can be easily constructed by adding more layers, with Λ increasing as $3.44n\sqrt{2}$ Å, but for the crystallographic description a division into the n odd and n even systems has to be made. For n odd the structure is described by the space

group D_{2h}^{19} (*Cmmm*, No. 65 in the International Tables[20]) with atoms in Wyckoff positions 2a and 2c. Increasing n, the extra layers occupy Wyckoff positions 4l and 4k, with the positional parameter z in increments of $(2n)^{-1}$. The n even systems lack inversion symmetry and thus have a horizontal glide plane instead of a horizontal mirror plane. These multilayers are described by the space group D_2^6 (*C*222, No. 21 in the International Tables[20]) with atoms in Wyckoff positions 4k. The first layer always has a positional parameter of $(2n)^{-1}$, and so there is no longer an atom in the origin. Figure 2(b), showing the NbZr 2:2 unit cell, together with its primitive translations, serves as an illustration of an n-even system.

The coherent multilayer structures, as used in the calculations, are described by only one atom per layer. Because the interlayer distance is constant, the space-filling Wigner-Seitz spheres were taken to have the same radii equal to $R_{ws}=1.694$ Å. They form a series of ideal multilayers, being square-wave modulated, with no lattice faults or interdiffusion across the interface.

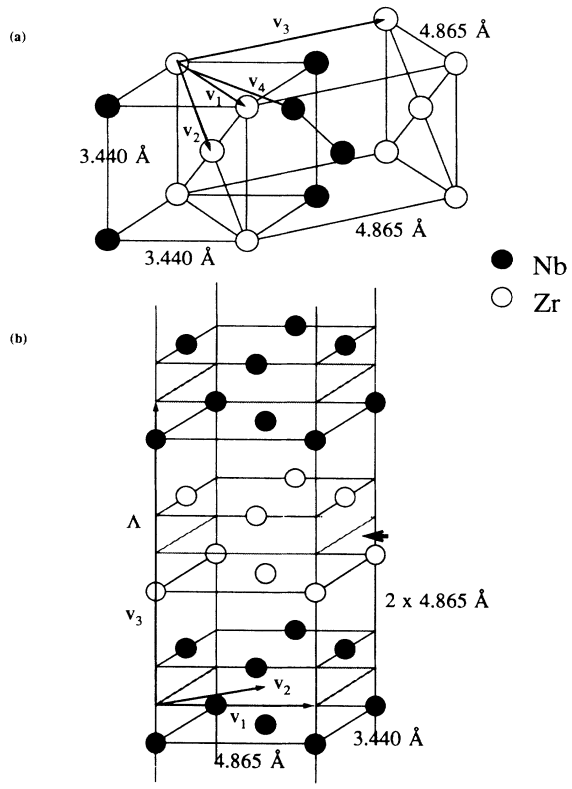

FIG. 2. The *C*-face-centered orthorhombic unit cell for a coherent Nb-Zr multilayer consists of Nb and Zr layers perpendicular to the bcc (110) direction. The NbZr 1:1 unit cell (a) is described by the basis vectors V_1, V_2, and V_3 with atoms in Wyckoff positions 2a (origin) and 2c. The vectors V_1, V_2, and V_4 are used in Sec. IV C as a definition of the bcc structure which emerges from this figure when all atoms are chosen equal. The NbZr 2:2 cell (b) serves as an example of the even-n multilayers. In these systems all atoms are in Wyckoff position 4k. (The arrow indicates the glide plane). The vectors V_1 and V_2 are the same as in (a), but V_3, which is along the modulation direction, increases as Λ.

For the incoherent ML no unit cell is reported. It is reported, however, that the Nb part of the ML is still bcc (110) modulated but that Zr now is hcp (002) modulated. From these observations we set out to derive a model for the incoherent ML system.

Two problems have to be solved in modeling an incoherent unit cell. The first one concerns the combination of Nb bcc (110) and Zr hcp (002) planes in an overall translational unit. The second one regards the positions of the interface atoms.

Although the individual layers do have two-dimensional translational symmetry, the lattice vectors are different. The projection of these layers in a plane will, in general, not exhibit commensurate translational symmetry. The problem is then to find lattice vectors for our incoherent system perpendicular to the modulation direction. To keep a limit on the computational effort we seek for vectors with the constraint that the total number of atoms inside the unit cell must be manageable.

In order to find the lattice vectors parallel to the layers, the layers were shifted with respect to each other such that one Zr atom was on top of a Nb atom. The Nb layer is described by centered rectangular cells of dimensions a_{Nb} and $a_{Nb}\sqrt{2}$. The Zr hcp layer is described by similar cells but with dimensions a_{Zr} and $a_{Zr}\sqrt{3}$. The angle between the short sides of the rectangles containing the atoms in the origin is defined as ϕ. The required lattice vectors of our incoherent cell are obtained if we find two linearly independent positions where also a Zr atom is on top of a Nb atom. We look for such positions by varying ϕ, while in addition the lattice constants a_{Nb} and a_{Zr} are chosen from a range of values to increase the flexibility of the searching procedure. The value of a_{Nb} is chosen within the range 3.300 Å of the metal to 3.454 Å of the Nb-Zr solid solution and a_{Zr} is chosen between the metallic value of 3.230 Å and the value 3.240 Å as measured[9] for the $\Lambda \geq 109$ Å ML. By rotating the Nb plane on top of the Zr plane, for $a_{Nb}=3.300$ Å, $a_{Zr}=3.234$ Å, and $\phi=0.434$ rad, the positions (8.2500, 2.3335) and (21.4500, 11.6673) are found for the Nb atoms as the best match. The coordinates of the corresponding Zr atoms are smaller by (0.0254, −0.0278) and (0.0009, 0.0018). After averaging these positions translational symmetry is described by the vectors $\mathbf{b}_1=(8.2371, 2.3473)$ and $\mathbf{b}_2=(21.4498, 11.6660)$. The orientation of the layers in this situation is depicted in Fig. 3. This unconventional unit cell was transformed into a more regular shape described by the vectors (1,0) and (−2,1) in the basis b_i. With $\mathbf{b}_1$ now chosen along the x axis the final translational vectors $\mathbf{b}_1$ and $\mathbf{b}_2$ perpendicular to the modulation direction are (8.5650, 0, 0) and (6.6957, 5.3409, 0). In this geometry of the layers there are five Zr atoms equally spaced along the longer diagonal and six Nb atoms parallel to the $\mathbf{b}_2$ axis at the origin and $\frac{1}{2}\mathbf{b}_1$. By the above-mentioned averaging of positions there are small deviations introduced in the in-plane nearest-neighbor distances, but without these small deformations, which are less than 0.03 Å, it was not possible to find a manageable unit cell. The present structure results in only $11n$ atoms in the unit cell of an incoherent NbZr $n:n$ multilayer. Layers other than interface layers are constructed ac-

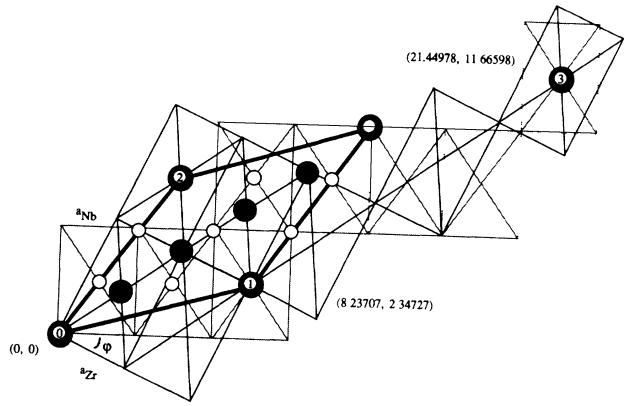

FIG. 3. To find the unit cell for the incoherent system, a Zr hcp (002) layer on top of a Nb bcc (110) layer is rotated by an angle ϕ. For $\phi=0.434$ rad, with $a_{Nb}=3.300$ Å and $a_{Zr}=3.234$ Å, the linearly independent positions 1 and 3 were found to coincide. This defines the vectors from the origin to these positions as lattice vectors. In the calculations the vectors from the origin to atom 1, now defined along the x axis, and to atom 2 are chosen to define the (x,y) plane of the unit cell. The atoms that lie inside the unit cell are indicated by open circles for Nb and shaded circles for Zr.

cording to the stacking of the layers in the parent metals Nb and Zr. This defines the interlayer distances and the positions of the atoms. The interlayer distance of Nb bcc (110) layers is $d_{Nb}=2.318$ Å and for Zr hcp (002) layers is $d_{Zr}=2.585$ Å derived from the average in-plane lattice distances and a c/a ratio for Zr of 1.593. The interface distance $d_{Nb\text{-}Zr}$ was taken as the average of the interlayer distances of Nb and Zr and consequently becomes 2.452 Å. The modulation wavelength Λ for the incoherent systems can now be defined as $n(d_{Nb}+d_{Zr})$. The Wigner-Seitz radii of the atoms in the incoherent system are determined to correspond as much as possible to the values they have in the parent metals. For the Nb and Zr atom the values for R_{WS} of 1.616 and 1.781 Å, respectively, were taken, to be compared with the metallic bulk values of 1.625 and 1.770 Å.

Up until now we have determined a commensurate unit cell for the Nb and Zr lattices. The phase between the two lattices is not determined yet. The question we address now is the determination of this phase factor together with the relaxation of the atomic positions at the interface. In actual systems the lattice mismatch can result in the creation of misfit dislocations,[21] and besides this a reordering of the interface can occur by interdiffusion and alloying.

In order to relax the Nb/Zr interface we used the following procedure. The interface is considered to be limited to the touching Nb and Zr layer only, being a total number of 11 atoms. The structure of the noninterface layers and the interlayer distances, including the interface layer distance $d_{Nb\text{-}Zr}$, are kept fixed. The interface atoms are allowed to move inside the fixed volume between the bulk layers. The degree of freedom to shift the Nb lattice in the (x,y) plane with respect to the Zr lattice is used to eliminate the starting geometry dependence of a relaxed interface. The displacement towards relaxation of the interface atoms was determined by the following expression which is based on ASA overlap:

$$\mathbf{R}_j'=\mathbf{R}_j+\sum_{i=1}^{N_{\text{overlap }j}}[\langle R_i^{WS}+R_j^{WS}-R_{ij}\rangle - \tfrac{1}{2}(dR_i+dR_j)]\hat{\mathbf{R}}_{ji} \ . \quad (12)$$

Herein $\mathbf{R}_j$ is the position of an interface atom, R_i^{WS} is the ASA Wigner-Seitz radius of the ith atom, and $\hat{\mathbf{R}}_{ji}$ is a unit vector pointing from atom i to atom j. The dR_i are the equilibrium (bulk) overlap distances of the ASA spheres. These distances are defined as $2R_i^{WS}-R_i^{NN}$, with R^{NN} the nearest-neighbor distance. The dR_i values are 0.389 and 0.339 Å for Nb and Zr, respectively. The parameter $N_{\text{overlap }j}$ gives the number of Wigner-Seitz spheres that overlap with atom j. The final positions of the atoms are obtained when the directional average of overlap distances, given by the second term in Eq. (12), vanishes. In this way the positions of the atoms at the interface are determined by the interatomic distances and coordination numbers of the parent metals. Here the information is used that all interatomic force data of the bulk materials have resulted in a bcc structure for Nb and a hcp structure for Zr with the corresponding nearest-neighbor distances. The factor in Eq. (12) in square brackets, which is only accounted for when positive, so only in a repulsive fashion, implies that the overlap distances $\langle R_i^{WS}+R_j^{WS}-R_{ij}\rangle$ must become equal to the (average) bulk overlap distances. This factor is zero for noninterface atoms. Equation (12) is used in a double loop over the interface atoms. In the outer loop the sums of the components of $\mathbf{R}_j'$ perpendicular to the modulation direction are determined to calculate the shift of the Nb layers, including the Nb interface atoms, with respect to the Zr layers, by which the forementioned degree of freedom is eliminated. Inside this loop Eq. (12) is used again to determine the new positions of the interface atoms. The periodicity of the unit cell was included in this procedure.

We examined three different starting geometries, resulting in two different final interface geometries. Two input cases, which are extreme as for the ASA overlap, the first with the Nb and Zr atoms directly on top of each other in the origin as in Fig. 3 (12.19% overlap of the volume of the smallest sphere involved in the overlap), and the second optimized by shifting the layers (9.10% overlap), resulted in an identical interface geometry. The interface has in this case a maximum overlap of 4.65%. A third input geometry was constructed by shifting the Zr layers such that the geometry of the interface layer coincides with the geometry of the original next-nearest interface layer. This resulted in a relaxed interface with 4.88% overlap. Apparently the input geometry dependence has not been eliminated completely. We have chosen in our calculations the relaxed interface with the smallest (4.65%) overlap. An ASA overlap that is too big leads to unphysical results. The maximum allowable value for this overlap depends on the crystal structure, but it can be as small as 10%.

The incoherent cell constructed in this way is a mono-

clinic cell and has the space group C_s^1 (Pm, No. 6 in the International Tables[20]) with only a mirror plane. The positions of the atoms of the incoherent NbZr5:5 multilayer system are given in relative coordinates in Table I. To see the results of the relaxation procedure the positions of the interface atoms can be compared with the positions of the corresponding bulklike atoms, which have the same (x,y) coordinates as the interface atoms before relaxation. From this comparison it is seen that the Nb atoms have moved more than the Zr atoms, which is because the bcc structure is more open than the hcp structure. This can also be seen in Fig. 4 where the interface and near interface atoms are projected in the (x,y) plane. The Zr interface atoms are in the centers of triangles formed by the near-interface Zr atoms, the positions they would have if there is no distortion. The Nb atoms, connected by lines in this figure, form a net that would have been rectangular in case of no distortion. Concerning the z coordinates of the interface atoms it can be noted that the Nb and Zr atoms on the average have repulsed each other. The undisturbed z coordinates are 0.1891 and 0.2891 for Nb and Zr, respectively, while their corresponding averages after relaxation are 0.1857 and 0.2905.

TABLE I. Positions of incoherent ML. The positions of the atoms in symmetry classes 7 up to 28 are pictured in Fig. 4.

	x	y	z	
1	0.0	0.0	0.0	Nb bulklike
2	0.0	0.3333	0.0	
3	0.0	0.6667	0.0	
4	0.5	0.1667	0.0	
5	0.5	0.8333	0.0	
6	0.5	0.5	0.0	
7	0.75	0.4167	0.0945	Nb intermediate
8	0.75	0.7500	0.0945	
9	0.25	0.2500	0.0945	
10	0.25	0.9167	0.0945	
11	0.25	0.5833	0.0945	
12	0.75	0.0833	0.0945	
13	0.9139	0.0971	0.1919	
14	0.9716	0.3791	0.1853	Nb interface
15	0.9402	0.7466	0.1829	
16	0.4525	0.2641	0.1816	
17	0.4811	0.9014	0.1891	
18	0.4252	0.6165	0.1830	
19	0.1952	0.0262	0.2883	Zr interface
20	0.0044	0.8226	0.2908	
21	0.3887	0.2277	0.2919	
22	0.6056	0.4146	0.2912	
23	0.7933	0.6345	0.2094	
24	0.1289	0.2937	0.3945	Zr intermediate
25	0.7289	0.8937	0.3945	
26	0.3289	0.4937	0.3945	
27	0.5289	0.6937	0.3945	
28	0.9289	0.0937	0.3945	
29	0.1956	0.0270	0.5	Zr bulklike
30	0.9956	0.8270	0.5	
31	0.3956	0.2270	0.5	
32	0.5956	0.4270	0.5	
33	0.7956	0.6270	0.5	

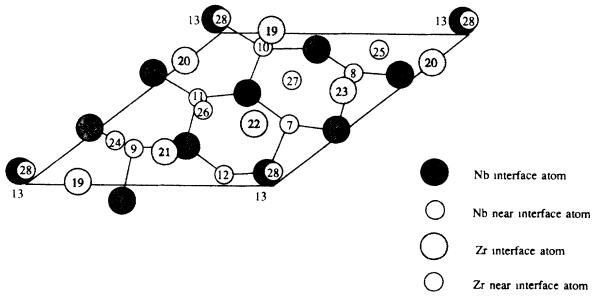

FIG. 4. Projection of the Nb and Zr atoms of the interface and near-interface layers on a plane perpendicular to the modulation direction. The atoms are numbered corresponding to the coordinates in Table I. The Nb atoms are connected by lines to guide the eye.

IV. RESULTS AND DISCUSSION

The coherent NbZr n:n multilayers were calculated for n ranging from 1 to 6. The largest modulation wavelength calculated consequently was 29.19 Å. Of the incoherent multilayers only the NbZr 5:5 system was calculated. The latter system has a modulation wavelength of 24.5167 Å. It contains 55 atoms in the unit cell, 11 atoms per n, whereas the coherent systems only have $2n$ atoms in each primitive cell.

In the calculations the scalar-relativistic Hamiltonian according to the description of Methfessel[22] was used. The exchange and correlation effects were treated by the local-density approximation using the Hedin-Lundqvist[23] parametrization. The self-consistent calculation was carried out including all core electrons.

Iterations were performed with the **k** points uniformly distributed in an irreducible part of the first Brillouin zone corresponding to a volume of Brillouin zone of the order of 10^{-5} Å^{-3}/**k**-point. For this density of **k** points the results of the self-consistent iterations for the coherent ML systems became density independent. It was kept fixed for all calculations. Self-consistency was assumed when the changes in the local partial charges in each atomic sphere decreased to the order of 10^{-4}. Next the partial densities of states were constructed by solving the Hamiltonian for the number of **k** points that corresponds with a volume per **k** point of 3×10^{-6} Å^{-3}. As sampling histograms, 300 channels with a width of 4.33 mRy were used. All calculations were performed on a Control Data Corporation Cyber-205 supercomputer.

In the construction of the LSW basis, the spherical waves were augmented by solutions of the Schrödinger equation indicated with the atomiclike symbols 5s, 5p, and 4d, corresponding to the valence levels of the parent metals. The internal l' summation of Eq. (4), used to augment the central Hankel function at surrounding atoms, was extended to $l'=3$, resulting in the use of 4f orbitals. The number of atoms inside the screening cluster, for the different positions in the different structures, varied between 15 and 19.

The calculations were performed non-spin-polarized.

Because in the coherent structure the Nb lattice constant is somewhat larger than in the pure metal, we have tested the coherent NbZr 2:2 system for a possible occurrence of magnetism. However, a nonmagnetic solution was obtained for the spin-polarized calculation in this case.

In subsequent sections we will present the density-of-states curves (IV A) and results for the density of states at the Fermi energy (IV B 1), total energies (IV B 2), charge transfer between the layers (IV B 3), and the electron energy bands (IV C).

A. Density of states

In Figs. 5–7 the density-of-states (DOS) results for the calculated coherent and incoherent multilayers are presented. All curves are plotted on the same horizontal and vertical scale, except the total DOS of the incoherent NbZr 5:5 ML, which has a vertical scale twice as large.

Total DOS results for the coherent multilayers are show in Fig. 5. The pictures correspond to increasing modulation wavelength. The nature of the DOS is typical for a transition metal in the bcc structure.[24] In all curves three broad peaks can be observed, labeled *A*, *B*, and *C* in the top curve. Peak *A* ranges from -3.5 to -1.5 eV, peak *B* from -1.5 to $+1.5$ eV, and peak *C* from 1.5 to about 6 eV. These peaks remain almost fixed in position on going from NbZr 1:1 to NbZr 6:6. The most pronounced differences are visible in region C. In NbZr 1:1 one high sharp peak is superimposed around 4.25 eV. This peak has disappeared in the other multilayers, where instead we see two other peaks steadily growing with Λ, one at 3.5 eV and one at 5 eV. Region *B* becomes more steplike on going to larger Λ. Region *A* is virtually constant in shape, height, and position relative to the Fermi energy over the entire Λ range regarded.

The incoherent total DOS of NbZr 5:5, depicted at the bottom of Fig. 5 in a somewhat enlarged scale, shows less structure. One still observes three regions of superimposed peaks, region *A* from -4 to -2 eV, region *B* from -2 to $+2.5$ eV, and region *C* from 2.5 up to 6 eV.

To understand the trends in the DOS curves of the coherent ML we performed calculations for Nb and Zr in the ML crystal structure given by a bcc cell with a lattice parameter of 3.44 Å, which will be denoted 1:0 and 0:1, respectively. The corresponding DOS curves are presented in Fig. 6(a) for Nb and Fig. 6(h) for Zr. Inset (b)–(g) in this figure are the six local DOS curves for the layers of the coherent NbZr 5:5 ML. Figures 6(b)–6(d) belong to the Nb monolayers of the ML and approach the Zr layers in that order. Figure 6(b) corresponds to the central Nb layer and Fig. 6(d) corresponds to the Nb interface layer. Figure 6(e) corresponds to the Zr interface layer and Fig. 6(g) to the Zr central layer. The 1:0 and 0:1 DOS curves are quite similar, but there are some important differences in the peak positions. Apart from a rigid shift, there is also a difference in bandwidths. If we

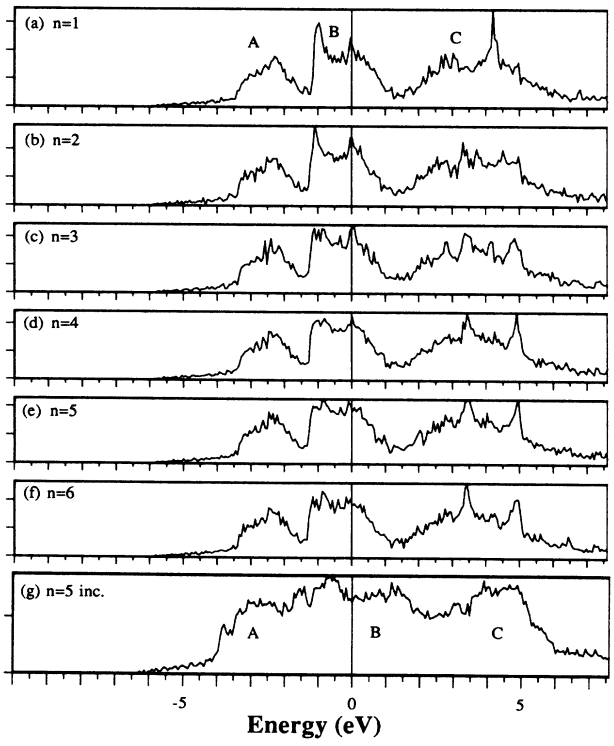

FIG. 5. Total DOS results for the coherent NbZr n:n multilayers for (a) $n=1$ to (f) $n=6$ and (g) the total DOS for the incoherent NbZr 5:5 multilayer. The latter curve has been scaled by a factor of 2 in the vertical direction with respect to the other DOS curves. The horizontal scale is in electron volts (eV) relative to the Fermi energy. The vertical scale is in arbitrary units.

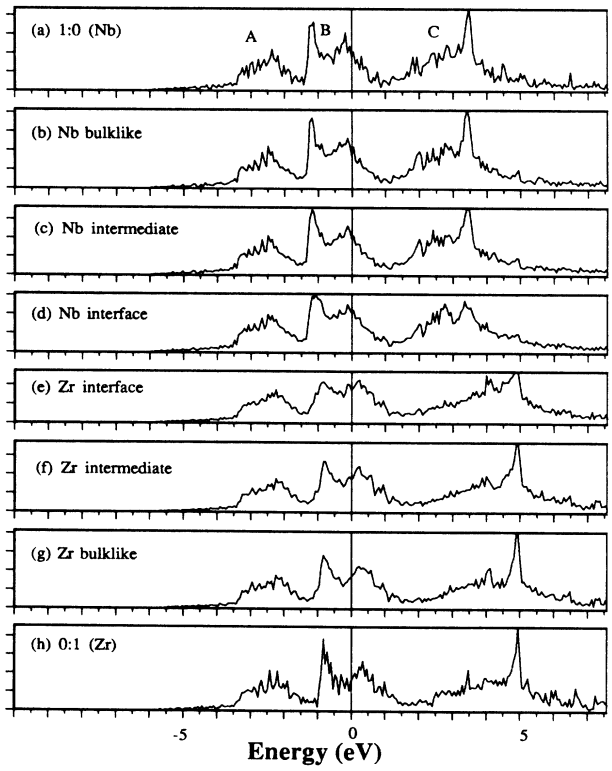

FIG. 6. Local DOS results for the coherent NbZr 5:5 multilayer (b)–(g), and results for (a) Nb and (h) Zr metals in multilayer bcc structures 1:0 and 0:1, respectively. Units as in Fig. 5.

label these curves as above for the total coherent DOS curves, peak *A* ranges from −3.5 to −1.5 eV for both 1:0 and 0:1, and peak *B* ranges from −1.5 to +1 eV for 1:0, and from −1 to +1.5 eV for 0:1. In region *C*, above about 2 eV the most important features are a peak at 3.5 eV for 1:0 and at about 5 eV for 0:1. We note that peak *A* is the same for 1:0 and 0:1, both in position and appearance. Peaks *B* are shifted in such a way that the maxima of Nb overlap with the minima of Zr.

It is seen that the curves for the Nb and Zr bulklike layers [Figs. 6(b) and 6(g), respectively] closely resemble the 1:0 and 0:1 curves which correspond to metallic bulk systems. In approaching the interface layers the DOS curves retain the features of the corresponding bulk systems, though they flatten gradually. The interface DOS curves are clearly flatter than the bulklike DOS curves and, apart from the differences in the *C* region, they get better matched to each other. The structure of the near-interface, intermediate, DOS curves is really in between that of the interface and bulklike DOS curves.

After these observations we return to the total DOS curves in Fig. 5. Using the rigid shift that is observed between the bulk 1:0 and 0:1 DOS curves, we now can explain the NbZr 2:2 to NbZr 6:6 DOS curves. Because peak *A* in Fig. 6 is independent of position with respect to the interface, its position is the same in the total DOS curves. The increasing steplike character of peak *B* in the total DOS curves can now be seen to be due to the rigid shift in peak *B* of 1:0 compared with 0:1. The extremes compensate each other and result in a flattening of peak *B*. The peaks at 3.5 eV and at about 5 eV can directly be related to peaks in region *C* of the 1:0 and 0:1 DOS. One can make an interesting observation of a Nb-Zr interaction by comparing the peaks for the 1:0, 0:1, and 1:1 systems. The 1:0 curve [Fig. 6(a)] has peaks at −1.25, −0.25, and +3.5 eV. The 0:1 curve [Fig. 6(h)] has peaks at −0.75, +0.25, and 5 eV. The 1:1 curve has its peaks exactly at the averages of these pairs of energy values, −1, 0, and 4.25 eV. These effects can be understood to a large extent by realizing that in the 1:1 system, which pertains to a system having interface only, the 1:0 and 0:1 layers have to match to a large degree, thereby reflecting the Nb—Zr bonding across the interface.

As for the coherent systems, we conclude that the DOS curves can be understood on the basis of the 1:0 and 0:1 curves alone. As a first step the 1:1 DOS is built from the 1:0 and 0:1 DOS. For larger modulation wavelengths the 1:1 DOS is simply mixed with the 1:0 and 0:1 DOS curves.

The incoherent DOS results are approached in the same way. As underlying calculations we now have to consider the bulk metals Nb bcc with lattice parameter $a=3.300$ Å and Zr hcp with $a=3.230$ Å and $c=5.145$ Å ($c/a=1.593$). The small changes in atomic distance as they occur in the multilayer are neglected in these metallic bulk calculations. The DOS results of the bulk metals are given in Fig. 7(a) for Nb and 7(h) for Zr. Insets 7(b)–7(g) display the summations of the local DOS of the atoms in a layer of the incoherent NbZr 5:5 multilayer in the same order as in Fig. 6. In comparing Figs. 7(a) and 6(a) the expected broadening of the *d* band is observed in

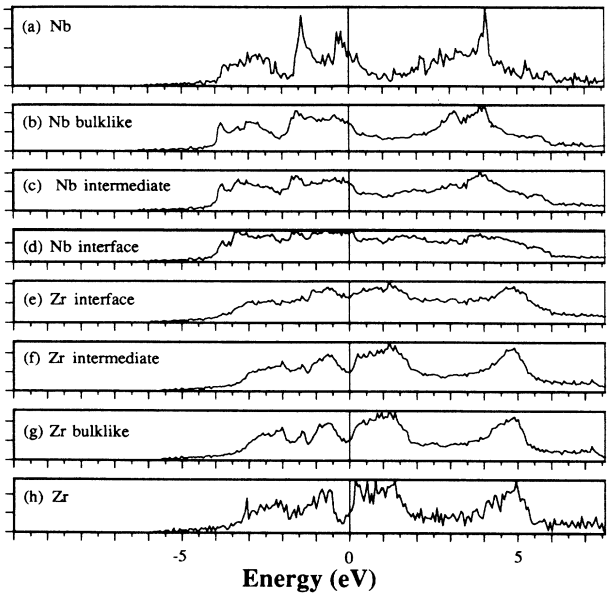

FIG. 7. Local DOS results for the incoherent NbZr 5:5 multilayer, (b)–(g) and results for the (a) Nb and (h) Zr metals. Curves (b)–(g) are the averaged local DOS curves for the atoms in the different layers. Units as in Fig. 5.

going to the bcc structure with the smaller lattice parameter. A marked change in DOS is observed for Zr in going from a bcc structure [6(h)] to a hcp structure [7(h)]. The first thing to notice in Fig. 7 is that the metals can be recognized in the bulklike layers. The Zr bulklike DOS [7(g)] resembles the metal DOS very well despite the additional fine structure in Fig. 7(h), which is partly caused by the fact that the **k**-point density used throughout the calculations is not optimal in this case. The comparison for Nb is still reasonable, although the bulklike DOS [7(b)] is considerably flatter. In approaching the interface layers, Zr almost retains its structure in the intermediate DOS curve. For Nb the curve becomes slightly flatter. In the Nb and Zr interface DOS curves, only faint details are left. For Zr there is still some similarity to the bulk DOS curve, but in the Nb interface DOS curve no characteristic Nb bulk features are left. This is not due to the summation over the atoms in a layer, because it is also observed for the DOS curves for the individual atoms in the layers.

The loss of structure of the DOS curves in going to the interface can be understood in terms of the interface geometry. Every interface atom, and a near-interface atom to a lesser extent, has a different atomic coordination, but the local geometrical differences could be more important than the chemical difference. The smaller effect of the chemical differences is illustrated by the behavior of the DOS curves for the coherent system (Fig. 6) in approaching the interface, for which system local geometry effects are absent by construction. An atom at the incoherent interface has an environment which resembles a disordered situation. Both the local distances and symmetries are different for these atoms. These differences induce splittings of states which are degenerate in more symmetric environments and consequently

lead to a smoothing of corresponding DOS curves. In fact, these results can be considered as a support for our rather simple procedure used to find an interface structure. A more sophisticated treatment of the relaxation could have resulted in somewhat different positions of the individual atoms, but would not have led to marked differences in the DOS curves. The forementioned structure of the incoherent total DOS curve [Fig. 5(g)] can now be seen as a superposition of the bulklike DOS curves on the steplike interface DOS curves.

In comparing the layer-resolved 5:5 results (Figs. 6 and 7) it is seen that for the incoherent ML it takes more layers to reach bulklike behavior. Further it can be seen that Zr will be the first component to approach bulklike properties. This has probably its reasons in the close-packed structure of Zr. During the relaxation of the interface, the Zr interface atoms were less flexible in moving than the Nb atoms. Also, the close-packed structure screens the interface more efficiently than a bcc (110) layer.

B. Numerical results

As numerical results of our calculations, we discuss the density of states at the Fermi energy, total and partial energies, and charge transfer across the interface.

1. Density of states at the Fermi energy

The density of states at the Fermi energy, $N(E_F)$, is determined from the DOS histogram by linearly interpolating between the $N(E)$ values at the two adjacent histogram channel energies. $N(E_F)$ in units of number of states per Rydberg and per atom is plotted in Fig. 8 as a function of Λ. The values for the coherent ML are connected to a curve, as is the $N(E_F)$ value for the incoherent ML with the coherent 4:4 value. These connections are only to guide the eye. We observe a decrease towards higher Λ, with a local maximum for NbZr 3:3. The $N(E_F)$ for the incoherent DOS lies well below the values of $N(E_F)$ for the coherent DOS.

The density of states at the Fermi energy can be compared with experimental results for two physical quantities that have been measured as function of Λ for the Nb/Zr ML system. These are the electronic specific-heat coefficient[8] γ given by

$$\gamma=\frac{\pi^2 k_B^2}{3}N(E_F) \tag{13}$$

and the superconducting transition temperature[9] T_c related to the $N(E_F)$ as

$$T_c=\frac{\Theta_D}{1.45}\exp\left[\frac{-1}{N(E_F)V}\right]. \tag{14}$$

The decrease, observed in Fig. 8, is consistent with experiment because both γ and T_c are measured to decrease with increasing Λ, but the measured decrease is much slower. After a decrease of $N(E_F)$ for small Λ, we observe a stabilization for larger Λ for the coherent systems. It is expected that $N(E_F)$ will converge to a constant

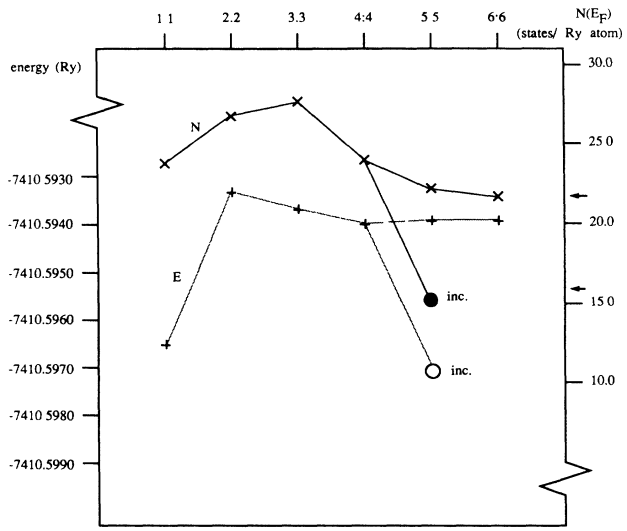

FIG. 8. Total energies in Rydberg per atom (+) and densities of states at the Fermi energy in units of number of states per Rydberg and per atom (×) for the different multilayers. The values of the incoherent multilayer are indicated by circles. The lines connecting the markers are to guide the eye. The average value of the density of states at the Fermi energy for the 1:0 and 0:1 systems is 21.7 and, for the metals, 15.9. These values are indicated by the arrows on the right.

value for larger Λ, which is supported by the layer-resolved $N(E_F)$ values given in Table II. With Λ, the number of bulklike layers increases, which will ultimately determine the multilayer $N(E_F)$. A similar behavior is expected for the incoherent system. This leads us to the following tentative interpretation of the measured Λ dependence of γ and T_c. For the measured samples considerable interdiffusion has been reported, which therefore have a much more extended interface than the systems calculated. This would imply that the slope of the decrease of γ and T_c with increasing Λ is much smaller than for the square-wave modulated systems investigated in this study. In this interpretation the NbZr 2:2 to 4:4 results in Fig. 8 are considered as representative for an interface region. The relative low $N(E_F)$ value of NbZr 1:1 will not be typical for an actual sample. It can be attributed to Nb—Zr bonding effects as mentioned in Sec. IV A, which for this solely interface system are free to develop. Lowe and Geballe[9] interpret their results in terms of a three-slices model. Their multilayers were considered to be built up from slices of Nb and Zr metal, separated by an interface slice containing a mixture of Nb and Zr. Apparently, this parametrized interpretation is supported by our self-consistent results for the density of states as a function of Λ.

The numerical value for γ is lower than the experimental value, which is 7.7 mJ/mol K^2 for $\Lambda=32.8$ Å. From the simple expression (13) the values for incoherent NbZr 5:5 and coherent NbZr 6:6 are 2.7 and 3.8 mJ/mol K^2, respectively. For comparison with experiment these values have to be corrected for electron-phonon enhancement anyhow. This enhancement factor is for Nb known[25] to lie between 1.8 and 2.0. Further, since for the mentioned

TABLE II. Layer-resolved $N(E_F)$ values (states/Ry atom).

Nb bulklike		Nb interface	Zr interface		Zr bulklike	
19.1					12.7	metals
16.7	16.4	18.1	15.5	12.2	12.9	incoherent ML 5:5
23.3	24.0	25.0	20.9	21.1	20.7	coherent ML 5:5
21.5	23.2	24.3	22.9	21.5	19.0	coherent ML 6:6
23.2					20.3	1:0,0:1

Λ the structure is still mainly coherent,[8] the second value of 3.8 mJ/mol K^2 can be considered as more representative than the first, lower value. Finally, in view of the more extended interface in the measured samples, another interface-induced enhancement of 10–20 % is expected from Fig. 8. Therefore, we conclude that our calculated density of states is in agreement with the experimental value of 7.7 mJ/mol K^2.

2. *Total energies*

Although we realize that the structural dependence of the total energies calculated by methods employing the ASA approximation have to be interpreted with care, we like to focus on some trends. From these we want to learn about the structural phase transition.

The total energies in Rydbergs per atom are depicted in Fig. 8. The numerical values are given in the bottom row of Table III. The energies of the coherent ML are connected to a curve, as is the energy value of the incoherent ML with the coherent 4:4 value. These connections are only to guide the eye. We first observe that the Λ dependence of the total energy is similar to that for $N(E_F)$. The saturation for the coherent system already starts at the NbZr 2:2 system, since the variations are in the 0.1 mRy range, which is of the order of the numerical error. The lower total energy for the incoherent system is consistent with a structural phase transition for larger modulation wavelengths. This can be supported by considering the layer-resolved total energies in Table III.

The energies of the interface layers are virtually constant for the coherent multilayers from NBZr 2:2 onwards. The pure-interface case, NbZr 1:1 shows a rise of the energy of the Nb interface atoms and a lowering of the Zr interface atoms compared with these constant values. For Nb all these values are higher than the 1:0 value and for Zr all values are lower than the 0:1 value. The energies of the incoherent ML interface layers follow the same rule, but the effects are more extreme. The near-interface values show a significant change towards the bulk values. The NbZr 3:3 values are slightly overcorrected, as are the values of the near-interface layers of the incoherent ML. From these data it is clear that the energies of the noninterface layers, being approximately constant, determine the total energy of the ML system. The average total energy of the coherent ML bulk systems (1:0 and 0:1), −7410.5945 Ry, being larger than the average of Nb bcc and Zr hcp, −7410.6015 Ry, shows that the incoherent ML structure is the preferred one, apart from possible interface effects. Since the average of the energies of the incoherent ML interface layers raises the total energy and the average for the coherent interface layers lowers the total energy, the coherent structure is expected to be the preferred one for small Λ. These conclusions, based on numerical results, are in support of the argument by Hilliard,[26] which can be summarized as follows. Everything but the interface for an incoherent ML is bulk, which is normally at an energy minimum. The interface raises the total energy, and this goes as the interface area per unit volume of ML, thus as Λ^{-1}. Since for an incoherent ML the interface is energetically unfavorable, the incoherent structure becomes less favorable with decreasing Λ. In this picture the interface effect for the coherent structure is negligible, since this

TABLE III. Energies per layer. In the first column the numbers in front of the decimal point are given. They are −7631 for the Nb atoms, −7189 for the Zr atoms, and −7410 for the total energies per atom in the bottom row. The total energy per atom for the incoherent ML was calculated using the fact that there are 30 Nb atoms and 25 Zr atoms inside the unit cell. The difference between the total energies and the summed energies per layer is the electrostatic energy due to deviations from charge neutrality, the Madelung energy.

	1:1	2:2	3:3	4:4	5:5	Incoherent ML	6:6	
−7631						0.6569	0.6464[a]	bulk Nb
					0.6437	0.6650	0.6438	bulklike
			0.6473	0.6453	0.6454	0.6637	0.6445	near interface
	0.6168	0.6362	0.6338	0.6346	0.6341	0.6037	0.6339	interface
	0.5689	0.5513	0.5550	0.5558	0.5551	0.5824	0.5557	interface
			0.5365	0.5403	0.5406	0.5367	0.5404	near interface
					0.5449	0.5338	0.5452	bulklike
−7189						0.5460	0.5426[a]	bulk Zr
−7410 (total per atom)	0.5965	0.5934	0.5937	0.5940	0.5939	0.5972	0.5939	

[a]Values for 1:0 and 0:1.

structure is formed by a distortion of layers to produce a lattice match at the interface. It is interesting to see from Table III that this effect is indeed small.

The drop of the total energy for the NbZr 1:1 system as seen in Fig. 8 can be understood in terms of an increased electrostatic interaction between Nb and Zr atoms due to an additional charge transfer. We will return to this in the next subsection. This effect will be smaller for the incoherent interface, due to the disordered positions of the atoms, so that the total energy for an incoherent NbZr 1:1 system will be larger than that for the coherent system, which is additional support for the observation that, for smaller Λ, coherence is preferred.

Although the results and conclusions are quite satisfactory, it should be kept in mind that, for the incoherent ML, distortions are introduced into the bulk parts. This can result in energy differences of the order of millirydbergs, which were not taken into account in the present study.

3. *Charge transfer*

The magnitude of the charge transfer between the different layers in the different systems is given in Table IV. A positive value indicates a decrease of electronic charge. It is observed that in all coherent systems the Nb interface atoms have attracted electrons, while in the incoherent system the Nb interface atoms have lost electronic charge. The charge transfer is a mechanism to align the Fermi energies of the parent metals. The potential of the dipole layer that arises will shift the Fermi energies to an overall Fermi energy.[1] The calculated Fermi energies for the 1:0, 0:1, and the bulk Nb and Zr systems explain the signs of the charge transfers. The Fermi energy of the 1:0 and 0:1 systems are -0.103 and 0.002 Ry, respectively. This means that electronic charge has to flow from Zr to Nb across the coherent interface to equalize the Fermi energies. The values for the Fermi energies of Nb and Zr are -0.025 and -0.053 Ry, which supports the opposite flow of electronic charge across the incoherent interface.

We want to point out that these self-consistent results for the relative shifts of the Fermi energies follow an intuitive rule, derived from the free-electron picture. Expansion or contraction of the lattice implies a decrease or an increase of the Fermi energy, respectively. This rule holds perfectly for simple metals, but for the more complicated transition metals exceptions could occur. In going from metallic Nb to the 1:0 system the lattice expands, and the Fermi energy decreases indeed. The volume per atom for Zr, measured in our description by the volume of the ASA sphere, decreases in going from metallic hcp Zr to the 0:1 system having the bcc structure, which is reflected by an increase in Fermi energy. So our self-consistent results can be considered as support for the intuitive rule, which apparently holds quite generally. Further, a decrease of the volume per atom intuitively implies a charge redistribution in favor of *d*-state charge at the cost of the more extended *s-p* labeled charge. According to our angular-momentum-projected results this rule is found to hold perfectly also.

A second thing to notice in Table IV is the damped oscillation around charge neutrality in going away from the interface. The charge transfer across the interface due to electronegativity differences of the constituent metals induces a dipole layer which is screened by Friedel-like oscillations. Furthermore, we notice that the charge transfer across the coherent interface is quite symmetric. The asymmetry at the incoherent interface is simply due to the different number of atoms in the two metallic layers. Finally, as already mentioned in the previous subsection, one clearly sees the relative huge charge transfer in the NbZr 1:1 system. In this system surrounding layers are not available to moderate the electronegativity effect.

C. Electron energy bands

In Fig. 9 the band plot is shown for the coherent NbZr 1:1 system along high-symmetry directions in the *C*-face-centered orthorhombic (cco) Brillouin zone (BZ), depicted in Fig. 12. In order to clarify the NbZr 1:1 band structure, the band plot for Nb in the ML crystal structure is given in Fig. 10. First we describe the relation between the bcc and cco Brillouin zones.

The basis of the bcc structure was chosen (column wise) as

$$\begin{bmatrix} b & b/2 & 0 \\ 0 & a/2 & a/2 \\ 0 & 0 & b/2 \end{bmatrix}$$

in order to have the (x,y) directions coincident with those of the cco structure. Here a is the bcc lattice constant and $b=a\sqrt{2}$. This basis is given by the vectors V_1, V_2, and V_4 in Fig. 2(a). The volume of this primitive cell is $ab^2/4$. This bcc cell has two basis vectors in common with the basis vectors,

$$\begin{bmatrix} b & b/2 & 0 \\ 0 & a/2 & 0 \\ 0 & 0 & nb \end{bmatrix},$$

TABLE IV. Average neutrality deviations per layer.

1:1	2:2	3:3	4:4	5:5	Incoherent ML	6:6	
				−0.0072	0.0074	−0.0029	bulklike Nb
		0.0217	0.0072	0.0120	−0.0232	0.0109	near interface
−0.1267	−0.0344	−0.0508	−0.0457	−0.0474	0.0584	−0.0471	interface
0.1267	0.0344	0.0514	0.0454	0.0470	−0.0644	0.0468	interface
		−0.0228	−0.0069	−0.0112	0.0209	−0.0101	near interface
				0.0064	−0.0063	0.0022	bulklike Zr

of the coherent $n:n$ ML unit cells. For $n=1$ these vectors are given in Fig. 2(a) as V_1, V_2, and V_3. The volume of this cell is $2n$ times the volume of the bcc cell. For the bases of the reciprocal lattice we find

$$\text{cco:} \begin{bmatrix} 0 & 1/b & 0 \\ 0 & 1/a & 2/a \\ 1/nb & 0 & 0 \end{bmatrix},$$

$$\text{bcc:} \begin{bmatrix} 0 & 1/b & 0 \\ 0 & 1/a & 2/a \\ 2/b & 1/b & 0 \end{bmatrix}.$$

In Fig. 12 the first Brillouin zones for cco with $n=1$, and for bcc are given in the same coordinate system. From this figure it is trivial to relate the cco bands to the bands of a bcc metal. For instance, the bands from Γ to N in bcc must be found in the presently no longer equivalent horizontal Γ-to-X direction and the vertical Γ-to-Z-to-Γ direction in the cco band plot. To illustrate this we compare the bands of Nb 1:0 (bcc, $a=3.44$ Å, Fig. 10) with those for NbZr 1:1 (Fig. 9). From the band plots all corresponding directions can be recognized. We can indeed recognize in the cco X-to-Γ direction along Σ the bcc bands from point H to Γ and from point N to P combined with its mirror image. Also, the cco bands from point Γ to X can be seen to consist of bcc bands from point Γ to N and from point N to H. The entire structure of the NbZr 1:1 ML bands can be mapped in this way with the bcc band structure. The higher the energy, the more delocalized the states. Consequently, above the Fermi energy there is some mixing of the bands which makes comparison with the Nb bands less trivial.

Band plots for NbZr $n:n$ systems with $n>1$ can be unraveled using the same procedure. To give an impression

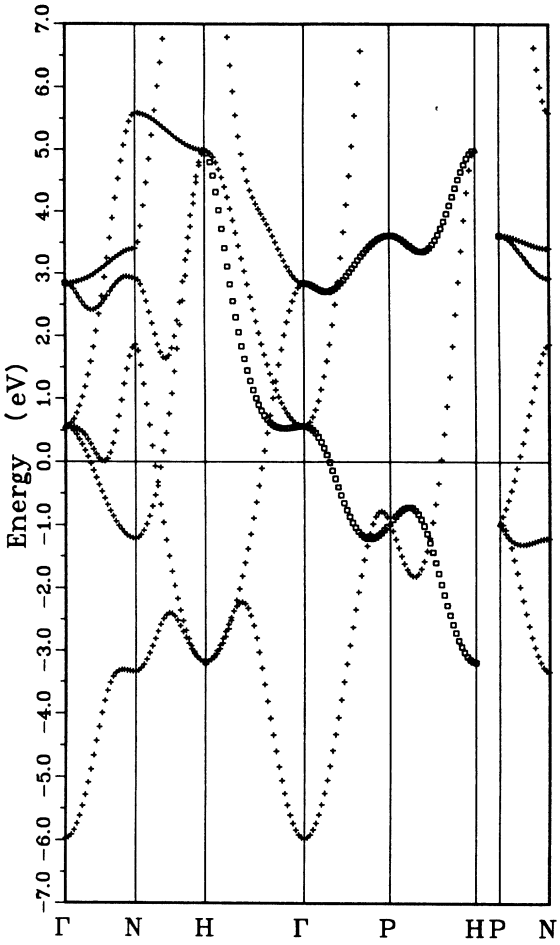

FIG. 10. Electron energy bands for Nb in the multilayer crystal structure (1:0), which is the bcc structure with lattice parameter 3.44 Å instead of the bulk value 3.30 Å. The squares in the figure indicate doubly-degenerate levels. The labels of the high-symmetry directions in the Brillouin zone of the bcc structure are presented in Fig. 12.

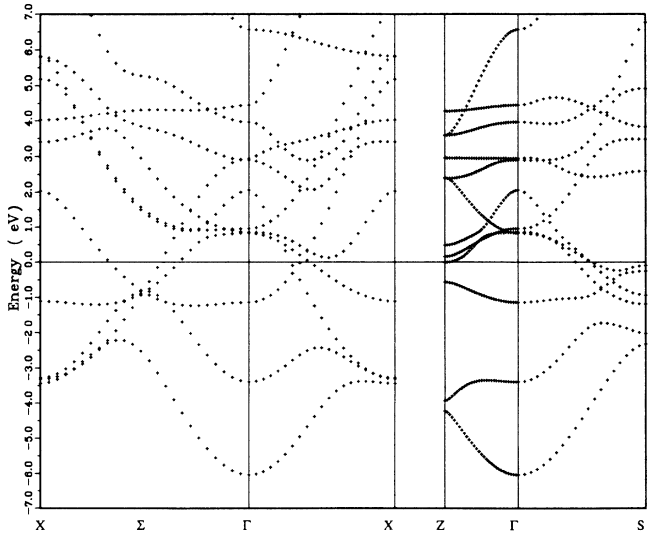

FIG. 9. Electron energy bands of NbZr 1:1 along directions in **k** space given in Fig. 12. The Γ-to-Z direction corresponds to the modulation direction of the multilayer.

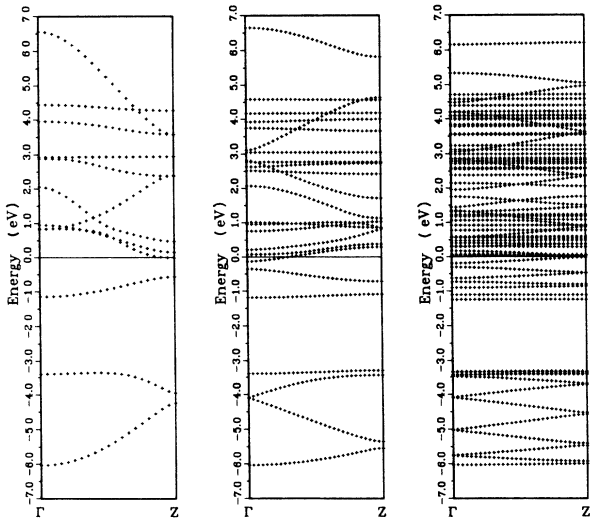

FIG. 11. Electron energy bands from Γ to Z for the coherent multilayers NbZr 1:1 (left), 2:2 (middle), and 6:6 (right). The k axes were chosen to be of the same length in the three pictures.

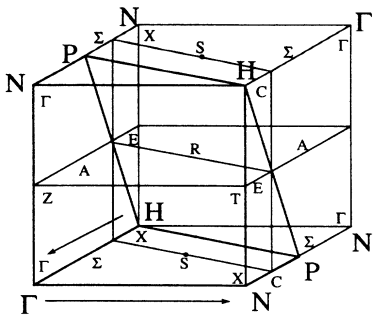

FIG. 12. The irreducible part of the bcc Brillouin zone, indicated by thick lines and large labels, drawn in coincidence with the cco Brillouin zone. The arrows indicate the direction along which the NbZr 1:1 bands of Fig. 9 are given.

of the increasing complexity with n, in Fig. 11 the band structures for $n=1$, 2, and 6 are given along the Γ-to-Z direction. The Γ-to-Z direction in the cco Brillouin zone is the direction in which the multilayering takes place. The bands in this direction are exclusively built out of the bcc bands along the Γ-to-N direction. For NbZr 1:1 this bcc direction is cut half-way by a horizontal plane according to Fig. 12. This results in a folding of the bcc bands and a potential splitting in the cco band plot at Z. In addition, in the NbZr 1:1 bands along the Γ-to-Z direction some hybridization effects can be seen around 3 eV. On going to higher n values, the effect on the band pictures can be understood by realizing that the length of the Γ-to-Z cco direction goes as $(nb)^{-1}$. This means the number of horizontal planes through the bcc BZ is $2n$. So now, beside the Γ-N-P-H plane, additional cross sections of planes through the cco Brillouin zone will be seen in the Σ-to-Γ-to-X direction and Γ-to-S cco directions. For the Γ-to-Z direction this means still further folding and potential splitting of the Γ-to-N bcc direction.

V. CONCLUSIONS

With electronic-structure calculations we have shown to be able to understand most of the experimentally observed properties of the Nb/Zr n:n multilayer system. The observed structural phase transition can be followed with our calculations by studying the layer-resolved total energies. The behavior of the density of states at the Fermi energy as a function of Λ matches with the observed trends in γ and T_c. From the band structures we can understand the effect of multilayering. The largest Brillouin zone, corresponding to the smallest Λ multilayer, gets sliced up in the modulation direction. In some cases this Brillouin zone can be related in a simple way to the BZ of the metallic components of the ML. The DOS curves of the coherent ML can be understood rather simply in terms of the DOS curves for the 1:0 and 0:1 structures. For the larger Λ multilayers the influence of the interface is observed to be diluted with bulk properties.

It should be kept in mind that the calculations are based on models for the multilayers. Interdiffusion was neglected by adopting sharp interfaces and the interlayer distances in all multilayers regarded were kept fixed. Due to a lack of experimental information the entire incoherent ML had to be modeled.

Still the results can be considered as satisfactory. In the near future the method will be applied to more complex metallic ML systems. The ultimate goal is to use it as a tool to predict new structures with unexpected, interesting, and useful properties.

Note added in Proof. After the submission of this paper, new measurements on the electronic specific-heat coefficient γ of the Nb/Zr multilayer system were published by Broussard and Mael.[27] Their results for $\Lambda=4$ and 22 Å, combined with previously obtained results,[8] form a curve having a maximum, just as our curve in Fig. 8 for the density of states at the Fermi energy does.

ACKNOWLEDGMENTS

Two of us (H.v.L. and A.L.) want to thank Professor R. Griessen and Dr. D. G. de Groot for helpful discussions. This work is part of the research program of the Stichting voor Fundamenteel Onderzoek der Materie (FOM), which is financially supported by the Nederlandse Organisatie voor Wetenschappelijk Onderzoek (NWO).

[1]M. L. Huberman and M. Grimsditch, Phys. Rev. Lett. **62**, 1403 (1989), and references therein.
[2]S. T. Ruggiero, Superlatt. Microstruct. **1**, 441 (1985).
[3]*Metallic Superlattices (Artificially Structured Materials)*, No. 49 of *Studies in Physical and Theoretical Chemistry*, edited by T. Shinjo and T. Takada (Elsevier, Amsterdam, 1987), see the appendixes.
[4]T. Jarlborg and A. J. Freeman, Phys. Rev. Lett. **45**, 653 (1980).
[5]T. Jarlborg and A. J. Freeman, J. Appl. Phys. **52**, 1622 (1981).
[6]F. Herman, P. Lambin, and O. Jepsen, Phys. Rev. B **31**, 4394 (1985).
[7]T. Oguchi and A. J. Freeman, J. Magn. Magn. Mater. **54-57**, 797 (1986).
[8]P. R. Broussard, D. Mael, and T. H. Geballe, Phys. Rev. B **30**, 4055 (1984).
[9]W. P. Lowe and T. H. Geballe, Phys. Rev. B **29**, 4961 (1984).
[10]T. Claeson, J. B. Boyce, W. P. Lowe, and T. H. Geballe, Phys. Rev. B **29**, 4969 (1984).
[11]A. R. Williams, J. Kübler, and C. D. Gelatt, Jr., Phys. Rev. B **19**, 6094 (1979).
[12]M. T. Czyżyk, R. A. de Groot, G. Dalba, P. Fornasini, A. Kisiel, F. Rocca, and E. Burattini, Phys. Rev. B **39**, 9831 (1989).
[13]R. A. de Groot, H. Gutfreund, and M. Weger, Solid State

Commun. **63**, 451 (1987).

[14]R. A. de Groot, in *Narrow-Band Phenomena—Influence of Electrons with Both Band and Localized Character,* edited by J. C. Fuggle, G. A. Sawatzky, and J. W. Allen (Plenum, New York, 1988).

[15]J. Ghijsen, L. H. Tjeng, J. van Elp, H. Eskes, J. Westerink, G. A. Sawatzky, and M. T. Czyżyk, Phys. Rev. B **38**, 11 322 (1988).

[16]M. Grioni, M. T. Czyżyk, F. M. F. de Groot, J. C. Fuggle, and B. E. Watts, Phys. Rev. B **39**, 4886 (1989).

[17]A. Messiah, *Quantum Mechanics* (North-Holland, Amsterdam, 1961), Vol. I, Appendix B.

[18]The question may be asked whether the desired degree of localization can be imposed by simply increasing the absolute value of the energy parameter κ. The use of a fixed energy parameter is discussed in Sec. II C of Ref. 11, where also the problem of the error in the eigenvalues associated with this approximation is addressed. The value of κ is set to the center of the energy range in which the eigenvalues are required. Alteration of κ by the additional requirement of localization will seriously affect the accuracy of the eigenvalues, more seriously the more localized functions are chosen. On the other hand, the localization procedure in the LSW method described in the main text does not influence the boundary conditions for the augmentation process at all and hence has no influence on the accuracy other than numerical convergence. In the case when the choice of one fixed value κ leads to errors over the energy range of interest which are unacceptable (i.e., the total-energy contribution of shallow core states to the eigenvalue spectrum of higher unoccupied states), one can extend the basis set by functions with different κ's and/or different number of radial nodes in augmenting function for both ASW and LSW methods. See, e.g., Ref. 12.

[19]O. K. Andersen and O. Jepsen, Phys. Rev. Lett. **53**, 2571 (1984).

[20]T. Hahn, *International Tables for Crystallography, Vol A: Space Group Symmetry* (Reidel, Dordrecht, 1983).

[21]J. P. Locquet, D. Neerinck, L. Stockman, Y. Bruynseraede, and I. K. Schuller, Phys. Rev. B **38**, 3572 (1988).

[22]M. Methfessel and J. Kübler, J. Phys. F **12**, 141 (1982).

[23]L. Hedin and B. I. Lundqvist, J. Phys. C **4**, 2064 (1971).

[24]V. L. Moruzzi, J. F. Janak, and A. R. Williams, *Calculated Electronic Properties of Metals* (Pergamon, New York, 1978).

[25]B. L. Gyorffy, in *Superconductivity in d- and f-Band Metals,* edited by D. H. Douglass (Plenum, New York, 1976).

[26]J. E. Hilliard, in *Modulated Structures,* Proceedings of the International Conference on Modulated Structures, Kailua Kona, Hawaii, 1979, edited by J. M. Cowley, J. B. Cohen, M. B. Salamon, and B. J. Wuensch (AIP, New York, 1979).

[27]P. R. Broussard and D. Mael, Phys. Rev. B **40**, 2321 (1989).

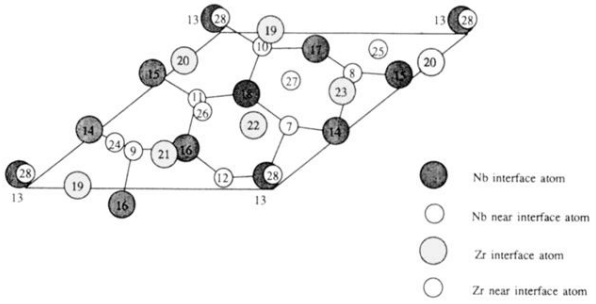

FIG. 4. Projection of the Nb and Zr atoms of the interface and near-interface layers on a plane perpendicular to the modulation direction. The atoms are numbered corresponding to the coordinates in Table I. The Nb atoms are connected by lines to guide the eye.